THE INFLUENCE OF FREESTREAM TURBULENCE ON THE TURBULENT KINETIC ENERGY BALANCE IN THE STAGNATION REGION OF A NORMAL FLAT PLATE

Michael Sherry*, **Robert Martinuzzi, David Wood**
Department of Mechanical Engineering
University of Calgary
2500 University Drive NW, Calgary, Alberta,
* msherry@ucalgary.ca

ABSTRACT

The turbulent kinetic energy balance is investigated in the stagnation region formed upstream of a flat plate subjected to two levels of freestream turbulence. This flow is of great interest as two-equation turbulence models such as $k-\varepsilon$, over predict turbulent kinetic energy production in the stagnation region, a phenomenon known as the *stagnation point anomaly*. Stereo particle image velocimetry is used to measure the mean and fluctuating velocity fields. The instantaneous pressure field is estimated from the velocity fields by an algorithm which solves the Poisson equation. The elevation of the freestream turbulence level by a passive turbulence grid significantly alters the turbulence properties in the stagnation region. The turbulent kinetic energy balance is dominated by the streamwise velocity component with production, P_k, almost exclusively arising from the streamwise normal stresses. The redistribution of turbulent kinetic energy among turbulence components was investigated via the pressure/velocity-gradient terms in the RANS equations.

INTRODUCTION

Flow past a bluff body results in a region of high strain in front of the body as the flow decelerates toward the stagnation point. Stagnation regions are thus found in every situation where a flow impinges perpendicularly to a solid surface. Atmospheric flow is turbulent and the effect of turbulence on the stagnation region is important in many industrial applications such as surface heat transfer beneath an impinging jet and wind loading of structures.

In this regard, investigations into the fluid dynamics of the stagnation region formed by axi-symmetric circular (Nishino *et al.*, 1996) and two-dimensional plane impinging jets (Guo & Wood, 2002; Sakakibara *et al.*, 1997) were motivated by industrial applications. Nishino *et al.* (1996) investigated the turbulent kinetic energy (TKE) balance in the stagnation region and found production of TKE was balanced by the coupled pressure-diffusion/dissipation term evaluated as a residual. Guo & Wood (2002) measured the fluctuating pressure field and came to a similar conclusion regarding the role of energy diffusion due to the pressure field. Guo & Wood (2002) also found a significant increase in streamwise normal stress levels close to the plate ($y/D \leq 1$, where D is the jet width) due to TKE production.

While axi-symmetric and plane jets are of interest in specialist industrial applications, the effect of freestream turbulence in the stagnation region of a two-dimensional bluff body has received little attention. This is despite the geometry's simplicity and analogous nature to many real world flows such as atmospheric boundary layer (ABL) flow impinging on a building surface. Further, interest in deployment of renewable energy devices such as wind turbines and photovoltaic modules on buildings in urban environments has increased with the advent of widespread use of Reynolds averaged Navier-Stokes (RANS) simulations to investigate these complex flow fields. Due to the high Reynolds numbers of the simulated flow field, a turbulence closure model is required. However, two-equation closure models, **e.g.** k-ε, suffer from an erroneous over-prediction of TKE in the stagnation region. This phenomenon is known as the *stagnation point anomaly* (Durbin & Pettersson Reif, 2011) and reduces the accuracy throughout the entire simulation domain. Several researchers (Durbin, 1996; Yap, 1987; Mohamed & Wood, 2015), have produced modifications to the k-ε model to minimise the over-prediction of TKE in the stagnation region. Mohamed & Wood (2015) recently compared several modifications to the k-ε model and illustrated improvements in the stagnation region of a building geometry were not necessarily replicated in the wake. This suggests the *stagnation point anomaly* is not confined to the production term, P_k of the TKE balance, shown in equation (1).

$$\begin{aligned}
&C_k + P_d + T + V_d + P_k + \varepsilon && = 0. \\
&-U_i \frac{\partial k}{\partial x_j} - \frac{1}{\rho} \frac{\overline{\partial u_i p}}{\partial x_i} - \frac{1}{2} \frac{\overline{\partial u_j u_j u_i}}{\partial x_i} && (1) \\
&+\nu \nabla^2 k - \overline{u_i u_j} \frac{\partial U_i}{\partial x_j} - \nu \overline{\frac{\partial u_i}{\partial x_j} \frac{\partial u_i}{\partial x_j}} && = 0.
\end{aligned}$$

where $k \equiv \frac{1}{2}\overline{u_i u_i}$ is the TKE. It is thus important to experimentally determine each term in equation (1) to allow assessment of more assumptions employed in the turbulence closure models. In equation (1), the terms are related to advection (C_k), pressure-diffusion (P_d), turbulent-transport (T), viscous-diffusion (V_d), production (P_k) and dissipation (ε).

To the authors' knowledge, there are currently no stagnation flow investigations of a finite width flat plate in which

the full turbulent kinetic energy and the normal stress budgets have been measured. The aim of the current manuscript is thus to investigate the effect of freestream turbulence on the TKE balance in the stagnation region of a flat plate model.

Experimental Setup

The experiments were undertaken in a 500 mm diameter suck-down open-type wind tunnel. The tunnel has a freestream turbulence intensity of 0.5% at 10ms^{-1}. To investigate the effect of freestream turbulence on the stagnation region, a passive turbulence grid was constructed and placed 336 mm upstream of the model. The uni-plane turbulence grid had a solidity, α, of 34%, a square 'bar' size, d, of 4.74 mm and a mesh length, M, of 25.4 mm. At the freestream velocity investigated, $U_\infty = 10 \text{ ms}^{-1}$, the grid elevated the three measured turbulence intensity components, $TI_i = \sqrt{\overline{u_i^2}}/U_\infty$, to 6.2%, 5.3%, and 5.7% for the streamwise, chordwise and spanwise directions respectively. The turbulence intensity levels illustrate the anisotropic nature at the model location. The integral length scale, λ_l, was determined by integrating the auto-correlation function of the fluctuating streamwise velocity component. This process resulted in a value of $\lambda_l = 25.5$ mm at the plate location in the empty tunnel. The low and high freestream turbulence intensity data-sets will be referred to as T1 and T2 respectively.

The experimental model was a machined flat plate with length, chord and thickness dimensions of $l = 534$ mm, $c = 29$ mm and $t = 1$ mm. The Reynolds number, based on U_∞ and c, was thus $Re_c = 19 \times 10^3$. The flat plate model spanned the entire wind tunnel jet, had an aspect ratio of 18.4 and is thus considered two-dimensional. The edges of the plate were precision machined into a $45°$ taper to ensure a fixed separation point. The surface of the plate was treated with a Rhodamine 6G solution to minimise reflections and improve reliability of the PIV vectors very close to the plate.

Stereo Particle Image Velocimetry (SPIV) was used to determine the velocity fields in the stagnation region of the model. Images were acquired by two high speed CCD cameras (SA4, Photron) fitted with Scheimpflug adapters and 100 mm macro lenses (AT-X PRO 100mm f/2.8, Tokina). A single cavity Nd:YLF 20 mJ pulsed laser (Photronics International, USA) with a wavelength of 527 nm produced a 1.5 mm thick laser sheet in the middle of the wind tunnel. A olive oil atomizer (model 9307, TSI) produced tracer particles with a mean diameter of 1μm. The two dimensional, three component (2D-3C) velocity vector fields ($\tilde{u}, \tilde{v}, \tilde{w}$) were determined by a commercial PIV software package (DaVis8, LaVision). A multi-pass cross-correlation algorithm was used with a final interrogation window size of 32 by 32 pixels with 50% window overlap applied. The resulting vector resolution was 0.64 mm. A single data set comprised of 2728 images recorded at a frame rate of $Fs = 500$ Hz resulting in a recording time of 5.45 s. Four data sets, $N = 10912$, were combined and temporally averaged together to investigate the mean (U, V, W) and fluctuating (u, v, w) fields.

The mean, P and instantaneous pressure fields, p, were estimated by an in-house code that integrates the Poisson equation using a second order central difference scheme (de Kat & van Oudheusden, 2012). Neumann boundary conditions were used along all edges of the domain. These were found directly from the Navier-Stokes equations in the appropriate direction. Dirichlet boundary conditions were applied at the two upstream corners of the domain by evaluating the unsteady Bernoulli equation at those points. Zero gauge pressure was assigned to the freestream velocity. The code was validated against direct numerical simulation data of the wake flow behind a 2D flat plate achieving good agreement.

Uncertainty in the mean turbulence quantities is evaluated at a 95% confidence interval using the formulae outlined in Benedict & Gould (1996). As the samples are considered correlated ($Fs > 1/2\lambda_t$), where $\lambda_t = \lambda_l/U_\infty$ is integral time scale (Benedict & Gould, 1996), N is reduced to an effective sample size, $N_{eff} = T_m/2\lambda_t$. The sample size is reduced to avoid unrealistically narrow confidence intervals (Benedict & Gould, 1996; Garcia *et al.*, 2006). Uncertainty in the pressure field is on the order of that of the mean velocity terms and uncertainty in k, is evaluated as the vector sum of each fluctuating component. As the uncertainty levels vary across the measurement domain, representative confidence intervals are shown in table 1. Errorbars in the figures represent the 95% confidence levels at that spatial location.

Table 1. 95% confidence intervals, as a percentage of the local value, in the approach flow ($x = 1.2, y = 0$) and in the stagnation region ($x = 0.1, y = 0$).

x, y	U	$\overline{u^2}$	$\overline{v^2}$	$\overline{w^2}$	$\bar{k}$	$\overline{u^3}$
1.2, 0	0.3	4.1	4.2	4.2	5.1	85.6
0.1, 0	3.3	7.2	5.5	4.9	8.3	17.2

A schematic of the experimental setup and the right-handed cartesian coordinate system (x,i: streamwise, y,j: chordwise, and z,k: spanwise) employed is shown in figure 1. Results obtained from the system described are presented in the following section.
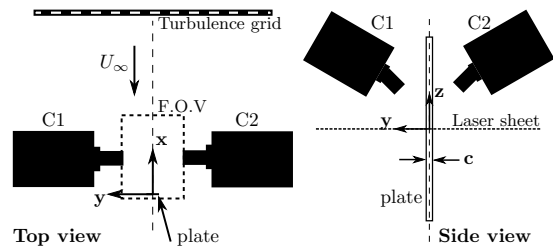

Figure 1. Top (left) and side (right) schematic views of the experimental setup. Schematic not to scale.

Results

The mean streamlines and streamwise velocity magnitude contours, U/U_∞, for the T2 data set are shown in figure 2. In the following figures, the velocity and length scales are made dimensionless by U_∞ and c respectively.
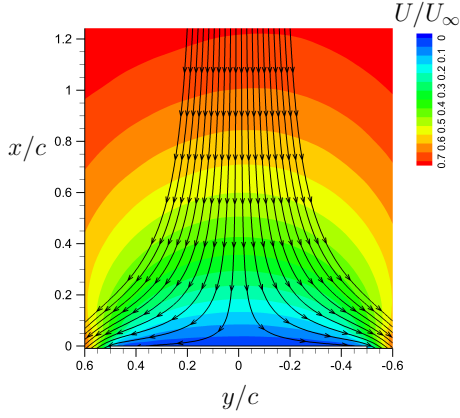
Figure 2. Streamlines and the normalised average streamwise velocity contours upstream of the flat plate for the T2 case.

Figure 3. Mean pressure field (gauge) produced by the flat plate in the T2 case.

Figure 2 illustrates the desired (for the purpose of investigating the TKE balance) deceleration of the mean flow toward the stagnation point. A slight asymmetry is visible due to the non-uniform anisotropic inflow generated by the turbulence grid. This asymmetry is absent in the low turbulence intensity case (not shown for brevity).

The mean pressure coefficient, $C_p = \frac{P - P_\infty}{0.5 \rho U_\infty^2}$, calculated from the instantaneous velocity fields is depicted in figure 2. The influence of the plate on the inlet flow can be clearly seen to extend beyond the current field of view. As the flow approaches the plate, the pressure (dynamic) reduces as the flow is decelerated. The dynamic pressure increases above unity at the plate edges as the flow is accelerated in the developing shear layers. Extracting the surface pressure on the plate reveals a maximum pressure coefficient at the stagnation point and decreases in the chordwise directions. The profile has a broader peak compared to infinite plate impinging jet flows (Guo & Wood, 2002) due to the finite width of the plate and is thus similar to that reported in Fage & Johansen (1927). The calculated pressure coefficient at the stagnation point differs from the theoretical potential value, $C_p = 1$ by -2.6% and -3.4% for the T1 and T2 cases respectively.

To investigate the *stagnation point anomaly*, the flow properties on the stagnation streamline are of primary interest. The normalised velocity components along the stagnation streamline for the two cases are shown in figure 5. In figure 5 and subsequent figures where both the T1 and T2 results are depicted, the solid lines represent the T1 results whereas the dashed lines and symbols represent the results for the T2 case. As the normalised strain field, S_{ij}, is equivalent between the two cases, the freestream turbulence intensity does not have a large impact on the mean velocities of the flow. The Heimenz (viscous laminar flow) solution (Schlichting, 1979) models the velocity potential in the stagnation region beneath the strained irrotational inflow with the linear functions, $U = -ax$ and $V = ay$. The streamwise (chordwise) velocity profiles vary linearly in the region $x/c < 0.2$ ($|y/c| < 0.15$). Sadeh *et al.* (1970*b*) also illustrated freestream turbulence does not influence the mean stagnation flow field upstream of an infinite width plate. Applying a linear fit to the streamwise velocity profile in the immediate vicinity of the plate, the stagnation constant a is estimated as ~ 1.01 (350s^{-1}) resulting in a viscous
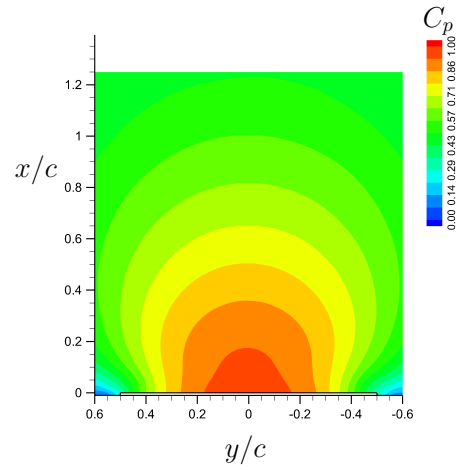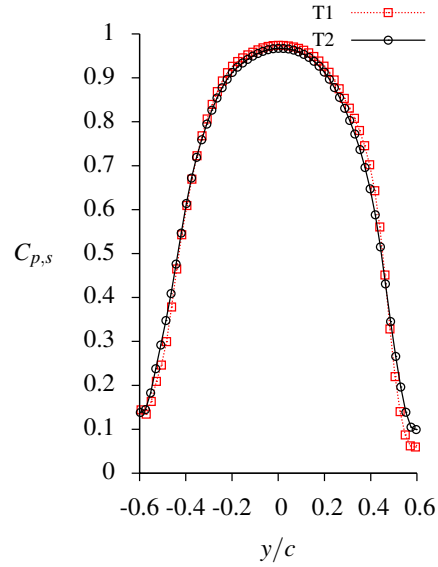

Figure 4. Mean surface pressure across the flat plate for both turbulent inflow cases.

boundary layer thickness of $\delta = 2.4 * (\nu/a)^{1/2} = 0.49$ mm. This result highlights the difficulty of resolving this layer and may serve as an explanation for the few experimental investigations to date. The neutral eddy length, $\lambda_0 = 2 * \pi * (a/\nu)^{-1/2} = 1.34$ mm, determined from the vorticity amplification theorem (Sadeh *et al.*, 1970*a*) suggests that the mean spanwise vorticity component, $\overline{\omega_z}$, in eddies generated by the grid $\lambda_0 \leq M \leq 25.4$ mm, could be amplified in the viscous boundary layer and lead to three dimensional (Görtler type) flow structures (Sadeh *et al.*, 1970*b*). However, both $\overline{\omega_z}$ and λ_0 are very small (especially on the stagnation streamline) in the current results and are thus not expected to have an effect on the TKE balance.

Reynolds averaging was performed on the instantaneous velocity fields to investigate the Reynolds normal and shear stresses along the stagnation streamline. The resolvable Reynolds stresses for $x/c < 0.6$ are shown in figure 6 for both turbulence cases. The freestream turbulence effecs
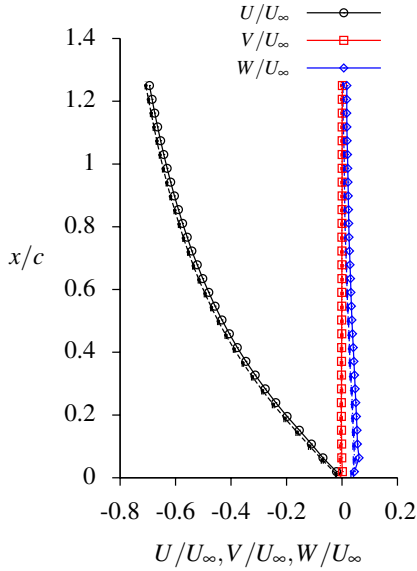
3

Figure 5. Normalised velocity components along the stagnation streamline for both turbulent inflow cases. Error bars represent the 95% confidence interval and every second data point is shown for clarity.
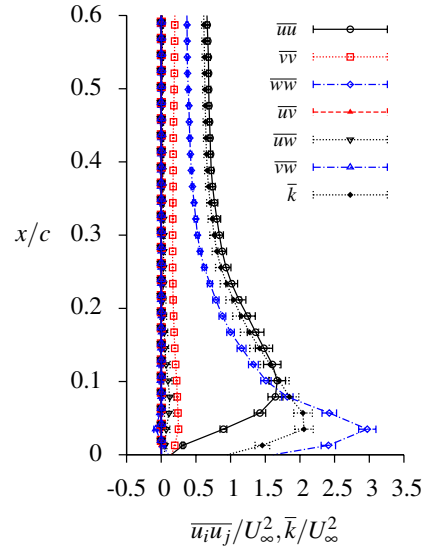

Figure 6. Normalised Reynolds normal, shear stresses and turbulent kinetic energy ($\times 100$) along the stagnation streamline for both turbulent inflow cases.

are immediately evident between the two cases. The T1 results are three orders of magnitude smaller than the T2 results and thus appear clustered on the vertical-axis. Conversely, the T2 results depict a highly anisotropic flow by the dominance of the streamwise normal stresses, $\overline{uu}$ across the majority of the domain, $x/c > 0.1$. This is unsurprising due to the minimal distance ($13M << 40M$) of the model downstream of the turbulence grid. This was intentional to model the anisotropic ABL flow past building surfaces. As highlighted by Mohamed & Wood (2015), the *stagnation point anomaly* can cause regions of negative normal stresses due to an inadequate eddy viscosity formulation in regions of high strain. This is unphysical by definition as supported by the current results.

The streamwise normal stress increases toward the plate due to turbulence production by the mean streamwise velocity gradient, *i.e.* due to the deceleration. The $\overline{uu}$ component peaks at $y/c \sim 0.15$ before being suppressed by the impermeability condition at the wall. The spanwise normal stress component, $\overline{ww}$ increases and exceeds $\overline{uu}$ beyond its peak close to the plate. A similar result was reported in a planar impinging jet investigation (Sakakibara *et al.*, 1997). The impermeability condition at the wall extends further into the flow than the no-slip condition causing $\overline{uu}$ to peak further from the plate compared to $\overline{vv}$ and $\overline{ww}$. Redistribution of turbulent energy among turbulence components occurs via pressure/velocity-gradient terms. Specifically, the pressure-rate of strain term, $\psi_{ij} = \frac{p}{\rho}\left(\frac{\partial u_i}{\partial x_j} + \frac{\partial u_j}{\partial x_i}\right)$, which appears in the Reynolds stress transport equations. From continuity, ψ_{ij} is traceless and hence does not appear in equation (1). However, it does have an important role in redistributing energy among turbulence components.

Using the in-house code to solve the Poisson equation for the instantaneous pressure field, ψ_{ij} was determined from the SPIV data. This term for the normal stresses, $\psi_{11}, \psi_{22}, \psi_{33}$, for both turbulence cases is shown in figure 7. The spanwise component, ψ_{33}, was estimated from the con-

tinuity relation, *i.e.* $\psi_{11} + \psi_{22} + \psi_{33} = 0$. The redistribution terms for the T1 case are much smaller than the T2 case and hence appear clustered on the vertical-axis. The streamwise redistribution term, ψ_{11} maintains a positive value throughout the domain indicating turbulent energy from $\overline{uu}$ is fed to the other components. A portion of this redistribution arises from the decay and return to isotropy of the generated turbulence. Close to the plate, wall reflections of the fluctuating pressure field will aid redistribution of turbulent energy from $\overline{uu}$ to the other components. ψ_{11} follows the form of the $\overline{uu}$ with a peak around $x/c = 0.15$. A slight increase in the chordwise normal stresses, $\overline{vv}$ occurs at this location (see figure 6) but the majority of energy is redistributed into the spanwise component as depicted by the decrease in ψ_{33} and increase in $\overline{ww}$ in figure 6. It should be noted that, as $\overline{uu}$ is damped by the impermeability condition near the wall, the flow remains anisotropic as shown in figure 6.

Figure 6 displays the dominance of the streamwise normal stresses; their influence on the TKE balance will now be investigated. To gain further insight into the exchange of TKE in the stagnation region, the six terms of the TKE balance introduced in equation (1) are considered.

It should be noted that the pressure-diffusion term is often coupled with the dissipation, ε in experimental velocimetry studies, **e.g.** (Nishino *et al.*, 1996). Guo & Wood (2002) showed the pressure-diffusion contribution to the TKE balance is non-negligible on the centreline of an impinging jet. The dissipation, ε, term in equation (1) could not be determined accurately with the spatial resolution of the current SPIV data. It is therefore determined as a residual in the TKE balance. P_k employed the continuity relation, *i.e.* $\partial W/\partial z = -\partial U/\partial x - \partial V/\partial y$, to determine the unknown spanwise gradient. The gradients of the triple products in the spanwise direction ($\partial \overline{wu^2}/\partial z$, $\partial \overline{wv^2}/\partial z$, $\partial \overline{w^3}/\partial z$) could not be determined from the current experimental setup. As the model is two-dimensional, they are assumed to be small and are thus ignored. Spatial derivatives are evaluated using a second order central difference scheme.
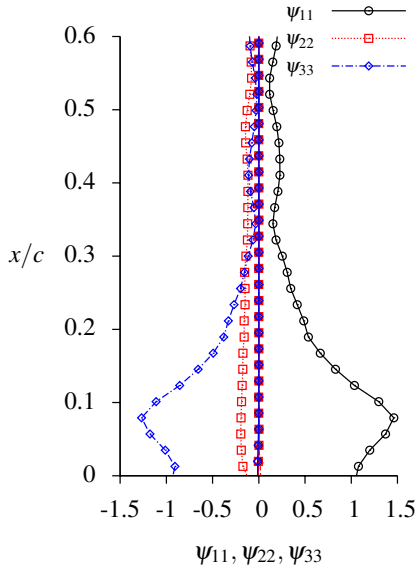
4

Figure 7. Pressure-rate of strain term ψ_{ij} ($\times 100$) on the stagnation streamline for both turbulent inflow case.
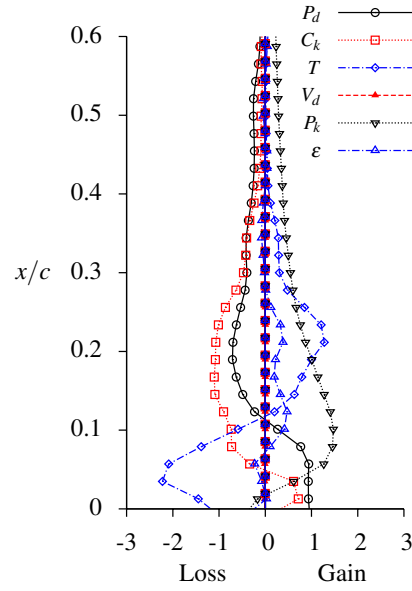

Figure 8. Normalised turbulent kinetic energy balance terms ($\times 100$) along the stagnation streamline for both turbulent inflow cases. See text body for description of terms.

The six terms in the TKE balance along the stagnation streamline are shown in figure 8 with a negative (positive) value representing a loss (gain) in the TKE balance. Production of TKE is primarily due to the straining of streamwise normal stresses, *i.e.* $\overline{uu}\partial U/\partial x$, with the peak in P_k corresponding to the peak in $\overline{uu}$ (**e.g.** see figure 6). The total production, P_k, also includes a smaller contribution from $\overline{vv}$ closer to the plate with a peak at $x/c = 0.05$. This production of TKE must be balanced by the diffusion terms, V_d, P_d and T and the advection of TKE throughout the domain. Of the diffusion terms, V_d, is an order of magnitude lower than the other terms and does not play a large role in the balance. However, pressure-diffusion acts to balance production prior to the peak of P_k. Below the maximum of P_k, P_d is approximately constant as the streamwise fluctuations, u, reduce linearly in the stagnation region.

The turbulent transport term, T also contributes heavily to the TKE balance and is dominated in a similar fashion to P_k by the streamwise velocity component. Transport of turbulent energy among components by the turbulence itself becomes increasingly important close to the plate. Approaching the plate, the impermeability condition at the wall causes a large gradient of the streamwise triple product, $-0.5 * \partial\overline{uuu}/\partial x$. Further, mixed triple products containing the spanwise component, (**e.g.** $\overline{w^3}, \overline{uw^2}$ etc.), increase T close to the plate as turbulent energy is redistributed to w by the pressure-rate of strain process (depicted in figure 7).

The dissipation, ε, of TKE is small throughout the investigated domain. This small magnitude and the fact it is evaluated as a residual in equation (1) highlights the difficulty in obtaining accurate dissipation measurements in the stagnation region. The experimental results allow investigation of the constant C_μ in the $k - \varepsilon$ definition of the eddy viscosity, $\nu_T = C_\mu k^2/\varepsilon$. The standard value of $C_\mu = 0.09$ was developed for free shear flows. To close the Reynolds shear stress equations, the $k - \varepsilon$ model represents the diffusive terms, P_d and T by a gradient transport model (Durbin & Pettersson Reif, 2011). The current experimental results (**e.g.** k in figure 6) indicate the predominant turbulent transport is in the streamwise direction. Thus

along the stagnation streamline, $P_d + T \sim \nu_T \partial k/\partial x$, which can be rearranged to solve for the constant. However, the small magnitudes of ε resulted in a C_μ estimate which varied greatly with spatial location. Alternatively, the diffusive terms, $(P_d + T)\varepsilon$ are compared to the estimate of the gradient transport model, $1/3(\partial k^3/\partial x)$ employed in the $k - \varepsilon$ closure model in figure 9. Approaching the region of high strain, the diffusive terms are much larger in the experimental results than the $k - \varepsilon$ gradient transport model would suggest. The gradient transport model using the standard value of $C_\mu = 0.09$ is also shown in figure 9 illustrating the lack of agreement in the stagnation region. It should also be noted that the stress-intensity ratio, $\overline{uv}/k$ along the stagnation streamline was an order of magnitude lower than the ratio used as a basis for the standard C_μ value. This result exemplifies the difference between this stagnation flow and a free shear layer and suggests an alternate value of C_μ is required for such stagnation flows.

Conclusions

This paper experimentally investigated the role of two inflows on the turbulent kinetic energy balance in the stagnation region of a flat plate. An anisotropic freestream turbulent inflow was generated by a passive turbulence grid. The instantaneous pressure field was estimated by an in-house code which solves the Poisson equation. The two cases were very different highlighting the impact freestream turbulence has on the stagnation region. In the high turbulence inflow case, the results highlighted the dominance of the streamwise velocity on the turbulent kinetic energy balance. The spanwise normal stress also increased dramatically close to the plate. The determined pressure-field accurately indicated the redistribution of turbulent energy from the streamwise normal stresses to the spanwise normal stresses. This redistribution process must be accurately represented in turbulence closure models. Further, the current results suggested the standard value of $C_\mu = 0.09$ used in $k - \varepsilon$ turbulence closure model was inadequate in the stag-
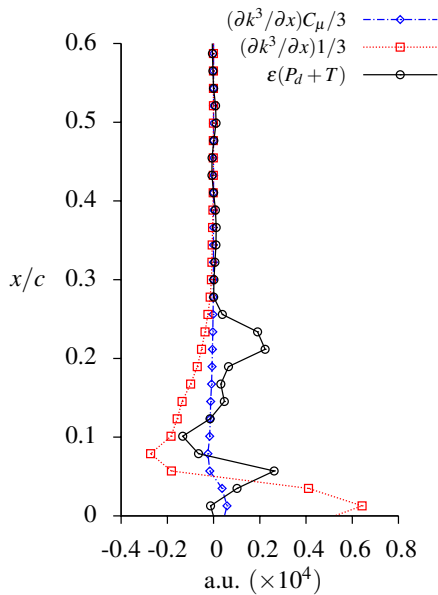
Figure 9. Terms contributing to the gradient transport model in the $k - \varepsilon$ turbulence model along the stagnation streamline for the turbulent inflow case.

nation region. The results provide a quality data set for turbulence model validation.

This research is part of a programme of work on renewable energy funded by the National Science and Engineering Council (NSERC). M.Sherry would like to thank P.Duplessix for access to the code to determine the fluctuating pressure field from the velocimetry data.

REFERENCES

Benedict, L. H. & Gould, R. D. 1996 Towards better uncertainty estimates for turbulence statistics. *Experiments in Fluids* **22**, 129–136.

de Kat, R. & van Oudheusden, B.W. 2012 Instantaneous planar pressure determination from piv in turbulent flow. *Experiments in Fluids* **52**, 1089–1106.

Durbin, P.A 1996 On the k-ε stagnation point anomaly. *International Journal of Heat and Fluid Flow* **17**, 89–90.

Durbin, P.A. & Pettersson Reif, B.A 2011 *Statistical theory and modeling for turbulent flows*. John Wiley & Sons.

Fage, A. & Johansen, F.C. 1927 On the flow of air behind an inclined flat plate of infintie span. *Proceedings of the Royal Society of London. Series A, Containing Papers of a Mathematical and Physical Character* **116** (773), 170–197.

Garcia, C. M., Jackson, P. R. & Garcia, M. H. 2006 Confidence intervals in the determination of turbulence parameters. *Experiments in Fluids* **40**, 514–522.

Guo, Y. & Wood, D.H. 2002 Measurements in the vicinity of a stagnation point. *Experimental Thermal and Fluid Science* **25**, 605–614.

Mohamed, M.A. & Wood, D.H. 2015 Modifications to the reynolds-averaged navier-stokes turbulence models for wind flow over buildings. *International Journal of Sustainable Energy* DOI: 10.1080/14786451.2015.1014903.

Nishino, K., Samada, M., Kasuya, K. & Torii, K. 1996 Turbulence statistics in the stagnation region of an axisymmetric impinging jet flow. *International Journal of Heat and Fluid Flow* **17**, 193–201.

Sadeh, W. Z., Sutera, S. P. & Maeder, P. F. 1970*a* Analysis of vorticity amplification in the flow approaching a two-dimensional stagnation point. *Journal of Applied Mathematics and Physics* **21**, 699–716.

Sadeh, W. Z., Sutera, S. P. & Maeder, P. F. 1970*b* An investigation of vorticity amplification in stagnation flow. *Journal of Applied Mathematics and Physics* **21**, 717–742.

Sakakibara, J., Hishida, K. & Maeda, M. 1997 Vortex structure and heat transfer in the stagnation region of an impinging plane jet (simultaneous measurements of velocity and temperature fields by digital particle image velocimetry and laser-induced fluorescence). *International Journal of Heat and Mass Transfer* **40**, 3163–3176.

Schlichting, H. 1979 *Boundary-Layer Theory*. McGraw-Hill.

Yap, C. R. 1987 Turbulent heat and momentum transfer in recirculating and impinging flows. PhD thesis, Faculty of Technology, University of Manchester, Manchester, UK.